Observation of cardiogenic flow oscillations in healthy subjects with hyperpolarized ^{3}He MRI

Guilhem J. Collier, Helen Marshall, Madhwesha Rao, Neil J. Stewart, David Capener, Jim M. Wild[*]

Academic Unit of Radiology, University of Sheffield, Royal Hallamshire Hospital, Sheffield, UK

Running Head: Observation of cardiogenic flow oscillations with HP ^{3}He MRI

[*]Correspondence to: Jim M. Wild, Ph.D., Academic Radiology, "C" floor, Royal Hallamshire Hospital, University of Sheffield, Glossop Road, S10 2JF, Sheffield, UK. Telephone: +44 114 226 5389. E-mail: j.m.wild@sheffield.ac.uk

Abstract:

Recently, dynamic MR imaging of hyperpolarized ^{3}He during inhalation revealed an alternation of the image intensity between left and right lungs with a cardiac origin (Respiratory Physiology & Neurobiology: 185, 468-471,2013). This effect is investigated further using dynamic and phase contrast flow MR imaging with inhaled ^{3}He during slow inhalations (flow rate ~ 100 mL s^{-1}) to elucidate air-flow dynamics in the main lobes in six healthy subjects. The ventilation MR signal and gas inflow in the left lower part of the lungs was found to oscillate clearly at the cardiac frequency in all subjects, whereas the MR signals in the other parts of the lungs had a similar oscillatory behavior but were smaller in magnitude and in anti-phase to the signal in the left lower lung. The airflow in the main bronchi showed periodic oscillations at the frequency of the cardiac cycle. In four of the subjects, backflows were observed for a short period of time of the cardiac cycle, demonstrating a pendelluft effect at the carina bifurcation between the left and right lungs. Additional ^{1}H structural MR images of the lung volume and synchronized ECG recording revealed that maximum inspiratory flow rates in the left lower part of the lungs occurred during systole when the corresponding left lung volume increased whereas the opposite effect was observed during diastole with gas flow being redirected to the other parts of the lung. In conclusion, cardiogenic flow oscillations have a significant effect on regional gas flow and distribution within the lungs.

Keywords: Cardiogenic oscillations, MRI, hyperpolarized gases, flow, lungs

Introduction

In the literature, the term cardiogenic oscillation has been used to refer to the modulation of the pulmonary gas pressure, flow or concentration produced by the cardiac cycle. Cardiogenic

2

36 oscillations have been intensively observed and recorded in the past in the context of pulmonary

37 physiology measurements made at the mouth with pressure transducers, pneumotachographs (1,

38 20, 29) or gas analyzers (6, 15) but also directly inside the intra-thoracic airways during

39 bronchoscopy (30). The cardiac cycle is thought to be an important component of gas mixing

40 within the lung (12, 13, 15) and leads to oscillations in the concentration of oxygen and carbon

41 dioxide in expired gas (5, 6). The cardiac action has therefore an uncontested influence on lung

42 function but it is unclear how the different observations of cardiogenic oscillations are related to

43 each other. In the present study, only cardiogenic flow oscillations (CO_f) present in the

44 conducting airways are considered. CO_f can be detected in most subjects during the whole

45 breathing cycle and in all regions of the lung (11). However, very little data has been published

46 on the influence of CO_f on airflow pattern and gas distribution within the lung.

47 On the other hand, the field of study of pulmonary airflow has recently benefited from

48 advancements in imaging and computation methodology. Computational fluid dynamics (CFD)

49 simulations using realistic image-based airway models have vastly improved general

50 understanding of the local characteristics of gas flow in the airways (25). These findings are of

51 particular interest for inhaled therapy research (4) or the study of regional deposition of particles

52 (17) but have yet to take into account realistic physiological features such as CO_f and have

53 traditionally relied only on validation with in vitro airway tree models (21). In vivo, rates of gas

54 ventilation in the main airways and the periphery can be assessed with dynamic hyperpolarized

55 (HP) [3]He ventilation imaging (16, 31). In addition, phase contrast velocimetry (PCV) sequences

56 can be used to directly map flow velocity profiles in the major airways (3, 10, 19). Sun et al. (24)

57 recently performed dynamic [3]He ventilation imaging on seven healthy subjects and revealed an

58 alternation of the MR image intensity between the left and right lung ("ventilatory alternans")

59 with a periodicity approximating the heart rate (unmeasured), which was presumably the effect

60 of cardiogenic flow oscillations. The aim of the present study is to further explore this

61 phenomenon by performing dynamic HP ^{3}He ventilation imaging during inspiration in healthy

62 subjects to assess the extent to which cardiogenic flow oscillations can influence the gas

63 distribution inside the lobes and, additionally, by measuring gas velocities inside the main

64 bronchi with PCV sequences to investigate the airflow pattern within the lungs.

Materials and Methods

65

Subject Characteristics, ^{3}He Production and Administration

66

67 Six healthy volunteers were recruited for this study (demographics and pulmonary function test

68 results shown in Table 1). Approval from the national research ethics committee was obtained

69 for all experiments. ^{3}He (Linde Gases, Huntingdon, UK) was polarized on site with a regulatory

70 approved spin exchange polarizer to ~ 25 % (GE Healthcare, Amersham, UK). A 1 L gas

71 mixture of N_2 and HP ^{3}He was delivered for the subjects to inhale inside the MRI scanner. The

72 subjects performed a slow and constant-rate inspiration (inhalation time varied from 8 s to 15 s

73 between subjects) from a Tedlar bag (Jensen Inert Products, Coral Springs, FL) containing 20 %

74 of HP ^{3}He for dynamic ventilation and 30 % for phase contrast velocimetry imaging. Data were

75 acquired during inhalation.

Image Acquisition

76

77 Imaging experiments were performed on a GE HDx 1.5T MR scanner with a maximum gradient

78 strength of 33 mT m^{-1} and slew rate of 120 mT m^{-1} ms^{-1}. A quadrature flexible transmit-receive

79 (T-R) ^{3}He radiofrequency coil (CMRS, Brookfield, WI) was used for dynamic ventilation and

80   1D velocity profile measurements. For 2D flow imaging across the left main bronchus, a home-

81   built dedicated loop-butterfly quadrature T-R coil with high quality factor ($Q_{loaded}/Q_{unloaded}$ ~

82   230/25) was used (see Fig. 1). The heartbeat of the subjects was monitored during all

83   experiments with a finger probe or an ECG. When ECG was available (see Table 1), the R-wave

84   occurrences were recorded during the imaging sequences. Sequence details were as follows:

85   -   Dynamic ventilation imaging: Dynamic coronal images of the 6 healthy subjects were

86   obtained with a spoiled gradient echo sequence (40×32 cm^2 field of view, 64 readout $\times$ 52

87   phase encode matrix, Cartesian sequential phase encoding, single slice, 25 cm thickness,

88   echo/repetition time T_E/T_R of 0.8/2.7 ms, $\pm$ 31.25 kHz bandwidth, 3° flip angle and 150

89   frames with a time resolution per frame of 140 ms).

90   -   1D velocity profile imaging: Axial 1D projections, across the anterior to posterior

91   direction, below the carina (see slice location 1, dashed line in the inset of Fig. 1) were

92   acquired in the 6 subjects with a PCV sequence, providing dynamic 1D velocity profiles

93   across the left and right main bronchi. A field of speed (FOS) of [-120, +120] cm s^{-1} was

94   chosen along the superior to inferior direction which is the principal direction of gas flow

95   (20 cm field of view, 128 points, 1 cm slice thickness, 20° flip angle and 768 frames with

96   a 20 ms time resolution).

97   -   2D flow imaging: A 2D oblique slice through the left main bronchus (see slice location 2,

98   solid line in the inset of Fig. 1) was imaged in subjects 1, 5 and 6 with a PCV sequence.

99   The field of speed was set to [-160, +160] cm s^{-1} in the direction of the axis of the left

100   main bronchus (5×3.75 cm^2 FOV, 32×18 matrix with a partial Fourier factor of 0.75 in

101   the phase direction and sequential Cartesian phase encoding, 1.5 cm slice thickness,

102   T_E/T_R of 3.3/6.4 ms, ± 15.63 kHz bandwidth, 18° flip angle and 232.4 ms time resolution

103   per image frame).

104   -   Cardiac gated proton lung imaging: In order to observe the deformation of the lungs

105   around the heart during the cardiac cycle, a standard cine cardiac gated balanced steady

106   state free precession ^{1}H pulse sequence was used to obtain an axial stack of images of the

107   lungs in the 6 subjects during breath hold (30 cm field of view, 256×256 matrix, 1 cm

108   slice thickness, 60° flip angle, T_E/T_R of 1.8/4.3 ms and 20 heart phases).

Image Analysis

110   For the dynamic ventilation images, four regions of interest (ROIs) in the Right/Left

111   Upper/Lower parts of the Lungs (RUL/LUL/RLL/LLL, see inset of Fig. 2A) were chosen and the

112   time evolution of the ^{3}He MR signal was computed in each. The mean signals in each ROI were

113   divided by the noise estimated from the first image of the experiment (acquired before inhaling

114   ^{3}He) to compute signal to noise ratio (SNR) values. A Fourier analysis was performed for each

115   SNR-time curve to detect the frequency of signal oscillations. The phase difference between

116   signals at the fundamental frequency was also computed (the phase of the LLL signal was taken

117   as a reference). Cardiac gated proton images were analyzed with ScanIP (Simpleware, Exeter,

118   UK) to segment the volume of the lung cavity for each of the twenty cardiac frames. Pulmonary

119   veins and arteries were not excluded. The relative volume changes ($V(t)/V_{mean}$) of the left and

120   right lungs around the heart during the cardiac cycle were derived from the segmentation.

121   For the PCV data, velocity maps and profiles were generated offline from the raw data using in-

122   house software developed in Matlab (MathWorks, Natick, MA). The phase difference

123   reconstruction was performed using the two interleaves of each frame to extract the ^{3}He gas

124 velocity component in the encoded direction for each pixel. ROIs corresponding to the left and

125 right main bronchi were selected manually and the time evolution of the average gas velocity

126 was calculated for each 1D profile. For the 2D flow imaging experiments, the flow was derived

127 by integrating the velocities over the area of the left main bronchus. An error analysis of the 1D

128 average gas velocity and 2D flow values was performed. The following formula gives the

129 statistical uncertainty of the velocity value derived from the phase difference reconstruction:

130 $$\sigma_v = \frac{FOS}{2\pi} \sqrt{(\sigma/S_1)^2 + (\sigma/S_2)^2} \tag{1}$$

131 where S_1 and S_2 are the magnitude values of the two interleaves and σ is the standard deviation

132 of the noise (the same in both interleaves). In practice $S_1 \sim S_2$ and the uncertainty in each velocity

133 value is therefore inversely proportional to the signal of each corresponding pixel. Since the

134 signal intensity is velocity dependent, the standard deviation of the velocity between pixels can

135 be fairly different. Indeed, the volume of gas in a pixel experiencing high flow rate is renewed

136 with "fresh" polarized gas (that has not undergone radio frequency destruction) more rapidly,

137 whereas pixels with low flow rate have lower signal and therefore higher variance σ_v^2. The

138 variance of the 2D flow measurement was calculated from the sum of each pixel variance

139 multiplied by the pixel area, whereas the variance of the 1D average velocity measurement was

140 derived according to the following formula:

141 $$\sigma_{av}^2 = \left(\sum_{ij}^{n} \sigma_{vij}^2\right)/n \tag{2}$$

142 where σ_{vij} is the standard deviation of the pixel ij and n is the number of pixels in the selected

143 ROI.

144

145 **Results**

146 Dynamic Ventilation: The signal to noise ratio (SNR) and hence, gas inflow in the left lower part

147 of the lung was clearly found to oscillate at the cardiac frequency in all subjects (see Fig. 2, Fig.

148 4, Table 2 and supplementary material for videos of dynamic ventilation images of each subject).

149 The signals in the other parts of the lungs (RLL, RUL and LUL) were also found to oscillate at

150 the same frequency in 5 of the 6 subjects, but with a markedly different phase when compared to

151 the LLL signal (139° was the average phase difference for the LUL signal, 167° for RLL and

152 145° for RUL). For subject 5 (Fig. 2F), no obvious pulsation was observed in the time evolution

153 of RLL, RUL and LUL SNRs. The simultaneous ECG recording in subjects 2, 3, 5 and 6 showed

154 that the R-wave occurrences corresponded to a minimum of SNR in the LLL (maximum SNR in

155 the other regions for subjects 2, 3 and 6) and were followed by a rapid rise of the LLL signal.

156 1D Velocity Profile: Although the experiments were performed during constant inhalation, the

157 average velocities in the left and right main bronchi fluctuated dramatically with a periodic

158 pattern whose frequency matched the heartbeat (see Fig. 3 and Fig. 4). The recorded velocities

159 ranged from -50 to 150 cm s^{-1} and varied antagonistically. More surprisingly, negative values

160 (backflows) were measured during a small part of the cardiac cycle in subjects 1, 3, 4 and 6,

161 demonstrating a pendelluft effect at the carina bifurcation between the left and right lungs.

162 Although the periodic patterns were quite different between subjects, recordings of R-waves

163 (start of systole) always preceded a strong gas inflow period in the left lung (low inflow or

164 backflow in the right lung) whereas the opposite phenomenon happened at the beginning of

165 diastole. The mean uncertainty in the measured average velocity value was found to be ± 6 cm s^{-1}

166 .

167 2D Flow: Measured velocity maps from the LMB confirmed the periodicity and dramatic change

168 of gas flow pattern during the cardiac cycle (see Fig. 5) and the existence of backflow in subjects

169 1 and 6. Flow values ranged from -40 to 220 mL s^{-1}. For subject 6, the ECG was recorded

170 simultaneously and the maximum flow rate into the left lung was observed after the R-wave

171 occurrence. σ_v was ~ 5 cm s^{-1} and the uncertainty on the flow values was below $\pm$ 2 mL s^{-1}.

172 Proton Imaging: Manual segmentation of left and right lung cavities surrounding the heart

173 exhibited a similar relative volume time evolution for all subjects (see Fig. 6 and online

174 supplementary material for a video of the lung segmentation of subject 1 through the cardiac

175 cycle). During systole, the segmented lung volume increased on average by about 53 mL, which

176 agrees well with the volume displaced per heartbeat of 60 mL quoted by Cotes et al. (5).

177 Interestingly, 83 % of this increase was found in the left lung. The volume contraction of the

178 heart ventricles corresponded to a left lower lung expansion confirmed by the displacement of

179 the pulmonary vasculature in the left lung around the heart (see online supplementary video).

180 During the first half of diastole, the opposite effect occurred with a similar rate of volume change

181 as during systole (see inset of Fig. 6). The second part of diastole did not show major lung

182 volume changes.

Discussion

184 In this study, a dramatic effect of cardiogenic flow oscillations on pulmonary airflow pattern was

185 observed in the lungs of normal subjects with functional ^{3}He MR imaging. Whereas Sun et al.

186 (24) noticed a 'ventilatory alternans' between the left and right lungs during inspiration in

187 healthy subjects, our data suggest that this observation is the consequence of stronger flow

188 oscillation in the left lower part of the lung due to the proximity of the heart, with accompanying

189 weaker oscillations of opposite phase in the rest of the lungs. We believe that Sun et al. did not

190 observe this localized origin most probably because of their choice of region of interest in the left

191   lung. The figure 1A of that study clearly shows that the left upper part of the lung was omitted in

192   the signal intensity calculation. However, the dynamic images from the subjects in that study

193   (available as videos in the online supplementary material) showed an alternans between the

194   upper and lower parts of the left lung. The increase in time resolution in the dynamic ventilation

195   imaging protocol between Sun et al. and the present studies (from 2.5 to 7.1 frames per sec) also

196   better facilitates the visualization of the alternans. Our data are also in agreement with previous

197   reports suggesting that the phase of CO_f is different in different parts of the lungs and that they

198   are more marked on the left side (30). Interestingly, the phase of the LUL signal seems to change

199   slightly in one subject (see Fig. 2A), which suggests that the phase difference between the lower

200   and upper parts of the left lung could depend on the lung inflation level in some cases. The signal

201   oscillations could be observed in all subjects in the LUL but only in 5 of 6 subjects in the rest of

202   the lungs. Similarly, the ventilatory alternans and the CO_f were observed in 5 of 7 subjects in the

203   imaging study of Sun et al. (24) and in 75 % of patients in a study by West et al. (30) with a gas

204   flow meter, which confirms that the existence and/or severity of CO_f are subject dependent.

205   However, it is worth noting that certain experimental and physiological conditions such as low

206   flow rates, hyperinflated lungs (13), higher cardiac output per beat and lower heartbeat

207   frequencies are more favorable for the observation of cardiogenic oscillations. Subject 5

208   performed a more rapid inhalation and had a faster heartbeat rate than the other subjects, which

209   could partly explain why no clear signal oscillations could be detected in the rest of that subject's

210   lungs.

211   In addition to dynamic ventilation imaging, the PCV MRI technique was developed to observe

212   the effect of cardiogenic oscillations on the gas flow in the left and right main bronchi, which

213   revealed the existence of a pendelluft effect. The ^{3}He gas velocity and flow values in the left and

214 right main bronchi were found to oscillate antagonistically and reversed backflows were

215 recorded in 4 of 6 subjects. The shape of the flow patterns, although having common features,

216 were different for all subjects. Among all subjects, the average velocity in both left and right

217 main bronchi during the cardiac cycle was about 38.7 cm s^{-1}. Assuming a Weibel cross section of

218 the airway with an area of 1.17 cm^2 for each main bronchus, and neglecting the fact that the slice

219 is not fully perpendicular to the bronchi directions (see slice location 1 in the inset of Fig. 1), an

220 average flow of 91 mL s^{-1} can be derived. This is roughly consistent with the expected average

221 flow of 85 mL s^{-1} deduced from the average time of 11.8 s that was required by the subjects to

222 inhale the 1 L bag of gas. PCV measurements have some limitations and possible scope for

223 improvements. It would be desirable to perform flow measurement at the entrance of the main

224 lobes and not only through the main bronchi, however, the localization of smaller airways is

225 highly challenging given the quality and resolution of MRI. In addition, in order to deduce the

226 exact flow pattern produced by CO_f, the measurement should also be repeated during breath

227 hold. However, because the ^{3}He signal is nonrenewable, fresh gas needs to flow constantly

228 through the ROI, which led us to a dynamic experiment during the inspiratory phase.

229 Nevertheless, estimates of maximum CO_f values in the left main bronchus can be obtained from

230 the 2D PCV measurements by inspection of the amplitude of the flow oscillations:

231 approximately 45 mL s^{-1} for subjects 1 and 5 and 70 mL s^{-1} for subject 6. These results are

232 reasonably consistent with previously reported volume flow rates of 42 mL s^{-1} (30). The addition

233 of simultaneous ECG recording with MR measurements showed that some features in the CO_f

234 pattern were common to all subjects. Maximum flow rates in the left lower part of the lung

235 occurred during systole whereas the opposite effect happened during diastole, with gas being

236 redirected to the other parts of the lungs.

237   The origin of CO_f has been a matter of debate for some time, stimulated by contradictory results

238   from different groups (11). Whereas early studies suggested an aspirating effect of the heart

239   during systole, simply explained by a pressure change induced by a volume change of the lung,

240   more recent works claim that CO_f are caused by pulmonary artery pulsatility (23, 29). It is

241   doubtful that pulmonary artery pulsatility could explain our observations of regional phase

242   difference between the left lower part and the rest of the lungs. Moreover the fact that these latter

243   studies are based on pressure and flow measurements at the mouth only, and were performed

244   during open chest conditions, raises the question as to whether the same, related or indeed

245   potentially different phenomena are being observed and compared. An alternative and more

246   satisfactory mechanism is given by Engel (11): the oscillatory motion of the heart, in addition to

247   volume changes, produces deflation and inflation in the surrounding parts of the lung, resulting

248   in a dynamic redistribution of the gas. It is clear from the segmentation of the cardiac gated

249   proton images that the mechanical action of the heart produces a volume change mainly affecting

250   the left lower part of the lungs (see Fig. 6 and online supplementary video); we believe that this

251   results in pressure changes causing the observed redistribution of gas within the lung. During

252   systole, the blood redistribution from the ventricles to the systemic and pulmonary circulation

253   results in a stretch of the left lower part of the lung. Simultaneously, more gas is observed to

254   flow into this part of the lung. During diastole, the heart volume increases at the expense of the

255   surrounding left lobe where expiratory flows are measured.

256   It is interesting to compare the proposed mechanism with recent models of pendelluft in the

257   bronchial tree (14). The pendelluft effect has been reported at different airway levels mainly in

258   pulmonary diseases or under abnormal conditions and is expected to occur when regions of the

259   lung have different dynamics of regional inflation and deflation (for example, regions with

12

260 different compliance and/or flow resistance due to lung disease). In this sense, the asymmetric

261 volume change created by the cardiac cycle could lead to regional pressure differences and

262 explain the pendelluft observed at the carina bifurcation, therefore reflecting the modelling

263 predictions by Greenblatt et. al. (14). However, the main difference in the observed pendelluft in

264 the present study is that it results from the natural cardiac motion in subjects with healthy lungs.

265 The resulting oscillatory gas flows constitute an additional mechanism for gas mixing in the lung

266 (12, 13, 15) but quantitative measurements are required to conclude on their significance. A

267 recent study supports that the heart-lung interactions are a vital source of gas mixing (26). In

268 addition, aerosol transport, mixing and deposition could be strongly affected by CO_f, which is

269 particularly relevant for inhaled therapeutics. Ma et al. (18) and Darquenne et al. (8) proposed

270 the existence of cardiogenic mixing to explain differences between measurement and simulations

271 of aerosol dispersion, and for the heterogeneity of particle deposition in microgravity,

272 respectively. In a following study, Darquenne et al. (7) addressed the effect of CO_f on the

273 deposition and dispersion of 1-μm particles during breath holds. Although gravitational

274 sedimentation is inferred to be the main mechanism, data have suggested that CO_f has a larger

275 effect in the central airways than in the periphery of the lung. We believe that the effect of CO_f

276 has been largely underestimated in the literature, especially in the field of CFD simulations of

277 airflow in the main airways (9, 17, 25), where the influence of the heart has not, to our

278 knowledge, been taken into consideration. Finally, it would be interesting to study how the

279 observed mechanism could contribute to the chaotic mixing of fine particles proposed by Tsuda

280 et al. (27). The classical theory assumes that acinar flow is kinematically reversible due to low

281 Reynolds number gas flow deep in the lung. However, Tsuda et al. (28) and Butler et al. (2)

282 observed kinematic irreversibility and complex convective stretch and fold patterns in excised rat

13

283 lungs supporting the theory that chaotic alveolar flow arising from flow trajectory asynchrony

284 governs aerosol transport and mixing in the lung periphery.

285 Further work to simulate the influence of CO_f on airflow patterns is required to supplement our

286 findings, but we hope this study will increase awareness of the effect of cardiac motion on gas

287 flow and distribution within the lungs among the pulmonary community.

288 Grants

293 Disclosures

294 No conflicts of interest, financial or otherwise, are declared by the authors.

295 References

296 1.   **Bijaoui E, Baconnier PF, and Bates JH**. Mechanical output impedance of the lung determined
297 from cardiogenic oscillations. J Appl Physiol (1985) 91: 859-865, 2001.
298 2.   **Butler JP, and Tsuda A**. Logistic trajectory maps and aerosol mixing due to asynchronous flow
299 at airway bifurcations. Respir Physiol Neurobiol 148: 195-206, 2005.
300 3.   **Collier GJ, and Wild JM**. In vivo measurement of gas flow in human airways with
301 hyperpolarized gas MRI and compressed sensing. Magn Reson Med (July 1, 2014). doi:
302 10.1002/mrm.25348
303 4.   **Corley RA, Kabilan S, Kuprat AP, Carson JP, Minard KR, Jacob RE, Timchalk C, Glenny
304 R, Pipavath S, Cox T, Wallis CD, Larson RF, Fanucchi MV, Postlethwait EM, and Einstein DR**.
305 Comparative Computational Modeling of Airflows and Vapor Dosimetry in the Respiratory Tracts of Rat,
306 Monkey, and Human. Toxicol Sci 128: 500-516, 2012.
307 5.   **Cotes JE, Chinn DJ, Miller MR, and Wiley InterScience (Online service)**. Lung function
308 physiology, measurement and application in medicine. Malden, Mass. ; Oxford: Blackwell Pub., 2006.
309 6.   **Dahlstrom H, Murphy JP, and Roos A**. Cardiogenic Oscillations in Composition of Expired
310 Gas - the Pneumocardiogram. J Appl Physiol (1985) 7: 335-339, 1954.

311   7.   **Darquenne C, Paiva M, and Prisk GK**. Effect of gravity on aerosol dispersion and deposition in
312   the human lung after periods of breath holding. J Appl Physiol (1985) 89: 1787-1792, 2000.
313   8.   **Darquenne C, West JB, and Prisk GK**. Deposition and dispersion of 1-micrometer aerosol
314   boluses in the human lung: effect of micro- and hypergravity. J Appl Physiol (1985) 85: 1252-1259, 1998.
315   9.   **De Backer JW, Vos WG, Vinchurkar SC, Claes R, Drollmann A, Wulfrank D, Parizel PM,**
316   **Germonpre P, and De Backer W**. Validation of computational fluid dynamics in CT-based airway
317   models with SPECT/CT. Radiology 257: 854-862, 2010.
318   10.   **de Rochefort L, Maitre X, Fodil R, Vial L, Louis B, Isabey D, Croce C, Darrasse L, Apiou**
319   **G, Caillibotte G, Bittoun J, and Durand E**. Phase-contrast velocimetry with hyperpolarized 3He for in
320   vitro and in vivo characterization of airflow. Magn Reson Med 55: 1318-1325, 2006.
321   11.   **Engel A**. Dynamic distribution of gas flow. In: Compr Physiol 2011, Supplement 12: Handbook
322   of Physiology, The Respiratory System, Mechanics of Breathing: 575-593. First published in print 1986.
323   doi: 10.1002/cphy.cp030332
324   12.   **Engel LA, Menkes H, Wood LD, Utz G, Joubert J, and Macklem PT**. Gas mixing during
325   breath holding studied by intrapulmonary gas sampling. J Appl Physiol (1985) 35: 9-17, 1973.
326   13.   **Engel LA, Wood LD, Utz G, and Macklem PT**. Gas mixing during inspiration. J Appl Physiol
327   (1985) 35: 18-24, 1973.
328   14.   **Greenblatt EE, Butler JP, Venegas JG, and Winkler T**. Pendelluft in the bronchial tree. J Appl
329   Physiol (1985) 2014.
330   15.   **Kelly SM, Brancatisano AP, and Engel LA**. Effect of cardiogenic gas mixing on arterial O2
331   and CO2 tensions during breath holding. J Appl Physiol (1985) 62: 1453-1459, 1987.
332   16.   **Koumellis P, van Beek EJR, Woodhouse N, Fichele S, Swift AJ, Paley MNJ, Hill C, Taylor**
333   **CJ, and Wild JM**. Quantitative analysis of regional airways obstruction using dynamic hyperpolarized
334   He-3 MRI - Preliminary results in children with cystic fibrosis. Journal of Magnetic Resonance Imaging
335   22: 420-426, 2005.
336   17.   **Lambert AR, O'Shaughnessy P, Tawhai MH, Hoffman EA, and Lin CL**. Regional deposition
337   of particles in an image-based airway model: large-eddy simulation and left-right lung ventilation
338   asymmetry. Aerosol Sci Technol 45: 11-25, 2011.
339   18.   **Ma BS, and Darquenne C**. Aerosol bolus dispersion in acinar airways-influence of gravity and
340   airway asymmetry. J Appl Physiol (1985) 113: 442-450, 2012.
341   19.   **Minard KR, Kuprat AP, Kabilan S, Jacob RE, Einstein DR, Carson JP, and Corley RA**.
342   Phase-contrast MRI and CFD modeling of apparent (3)He gas flow in rat pulmonary airways. J Magn
343   Reson 221: 129-138, 2012.
344   20.   **Montmerle S, and Linnarsson D**. Effects of gravity and blood volume shifts on cardiogenic
345   oscillations in respired gas. J Appl Physiol (1985) 99: 931-936, 2005.
346   21.   **Mylavarapu G, Murugappan S, Mihaescu M, Kalra M, Khosla S, and Gutmark E**.
347   Validation of computational fluid dynamics methodology used for human upper airway flow simulations.
348   J Biomech 42: 1553-1559, 2009.
349   22.   **Quanjer PH, Stanojevic S, Cole TJ, Baur X, Hall GL, Culver BH, Enright PL, Hankinson**
350   **JL, Ip MS, Zheng J, and Stocks J**. Multi-ethnic reference values for spirometry for the 3-95-yr age
351   range: the global lung function 2012 equations. The European respiratory journal 40: 1324-1343, 2012.
352   23.   **Suarez-Sipmann F, Santos A, Peces-Barba G, Bohm SH, Gracia JL, Calderon P, and**
353   **Tusman G**. Pulmonary artery pulsatility is the main cause of cardiogenic oscillations. J Clin Monit
354   Comput 27: 47-53, 2013.
355   24.   **Sun Y, Butler JP, Ferrigno M, Albert MS, and Loring SH**. "Ventilatory alternans": a left-right
356   alternation of inspiratory airflow in humans. Respir Physiol Neurobiol 185: 468-471, 2013.
357   25.   **Tawhai MH, and Lin CL**. Airway gas flow. Compr Physiol 1: 1135-1157, 2011.
358   26.   **Thurgood J, Dubsky S, Henon Y, Jesudason E, and Fouras A**. Heart-lung interactions: A vital
359   source of gas mixing within the lungs. Am J Respir Crit Care Med 189: A6275, 2014.
360   27.   **Tsuda A, Laine-Pearson FE, and Hydon PE**. Why chaotic mixing of particles is inevitable in
361   the deep lung. J Theor Biol 286: 57-66, 2011.

362   28.   **Tsuda A, Rogers RA, Hydon PE, and Butler JP**. Chaotic mixing deep in the lung. P Natl Acad
363   Sci USA 99: 10173-10178, 2002.
364   29.   **Tusman G, Suarez-Sipmann F, Peces-Barba G, Climente C, Areta M, Arenas PG, and**
365   **Bohm SH**. Pulmonary blood flow generates cardiogenic oscillations. Respir Physiol Neurobiol 167: 247-
366   254, 2009.
367   30.   **West JB, and Hugh-Jones P**. Pulsatile gas flow in bronchi caused by the heart beat. J Appl
368   Physiol (1985) 16: 697-702, 1961.
369   31.   **Wild JM, Paley MN, Kasuboski L, Swift A, Fichele S, Woodhouse N, Griffiths PD, and van**
370   **Beek EJ**. Dynamic radial projection MRI of inhaled hyperpolarized 3He gas. Magn Reson Med 49: 991-
371   997, 2003.

372

373   # Figure Captions
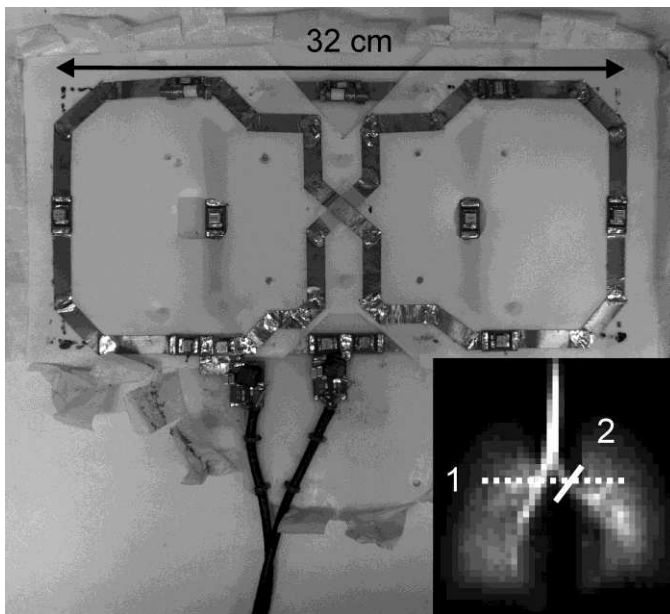
374

375   Figure 1:

376   Picture of the quadrature transmit/receive radiofrequency coil used for 2D flow measurement in

377   the left main bronchus (see slice location 2, solid line in the inset). Inset: example of a HP ^{3}He

378   ventilation image with indication of slice locations used for 1D (1) and 2D (2) phase contrast

379   velocimetry sequences.
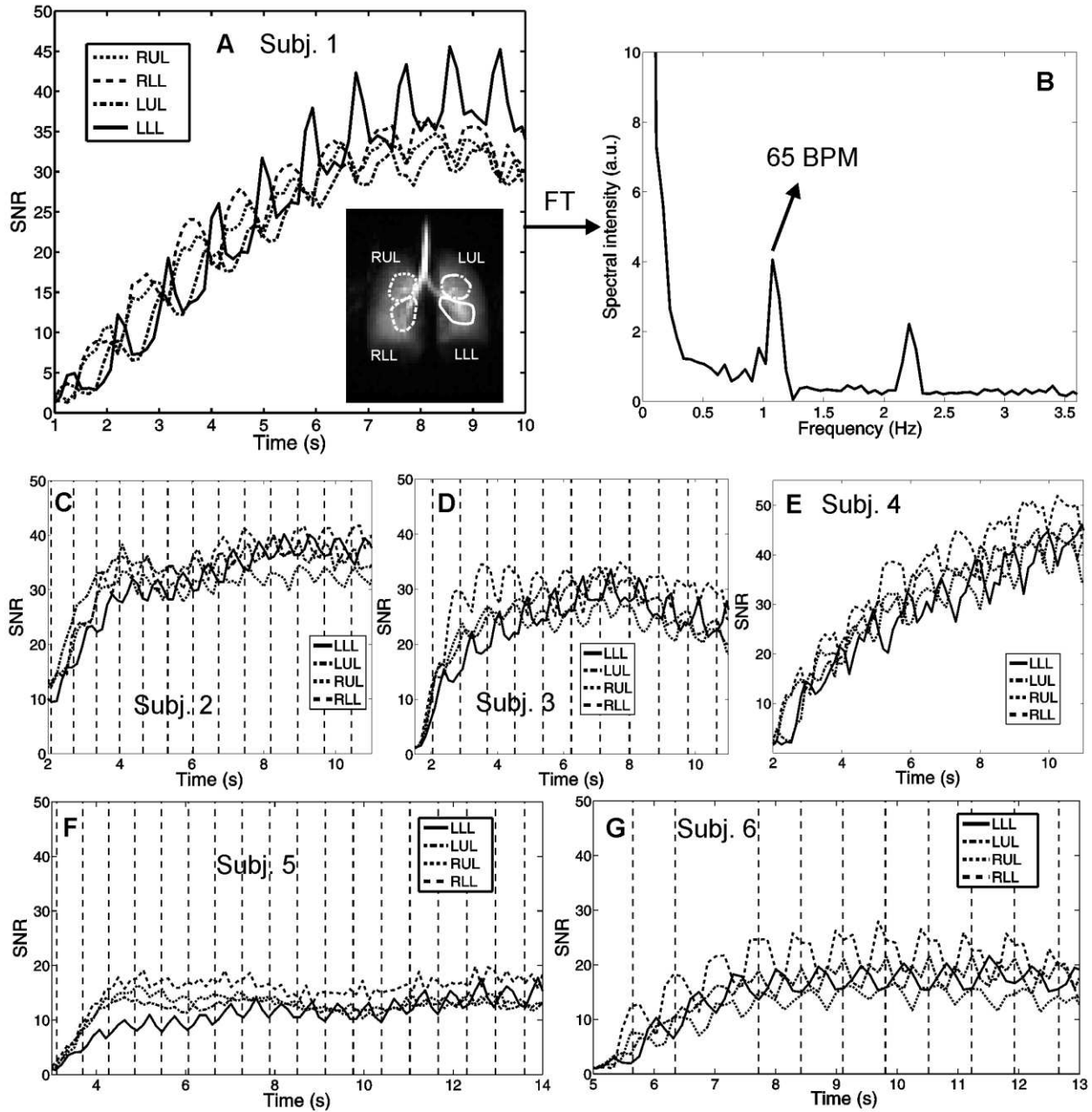
380

381   Figure 2:

382   **A**: Time evolution of the SNR in the 4 ROIs (RUL, LUL, RLL and LLL) of the Cartesian

383   dynamic images of subject 1 (example image and ROI positions shown in the inset). **B**:

384   Frequency spectrum of the signal corresponding to the left lower part of the lung (curve LLL in

385   **A**) after a Fourier transform (FT). The peaks at 1.08 and 2.2 Hz correspond to the fundamental

386 and the second harmonic of the heart rate of the subject (65 BPM). **C** to **G**: Time evolution of the

387 signal in the 4 ROIs for subjects 2 to 6. For subjects 2, 3, 5 and 6 the ECG was recorded and the

388 dashed vertical lines correspond to the occurrence of R-waves. Note: an R-wave occurrence is

389 missing (not recorded) in G (subject 6) at ~ 7 s.

390

391 Figure 3:

18
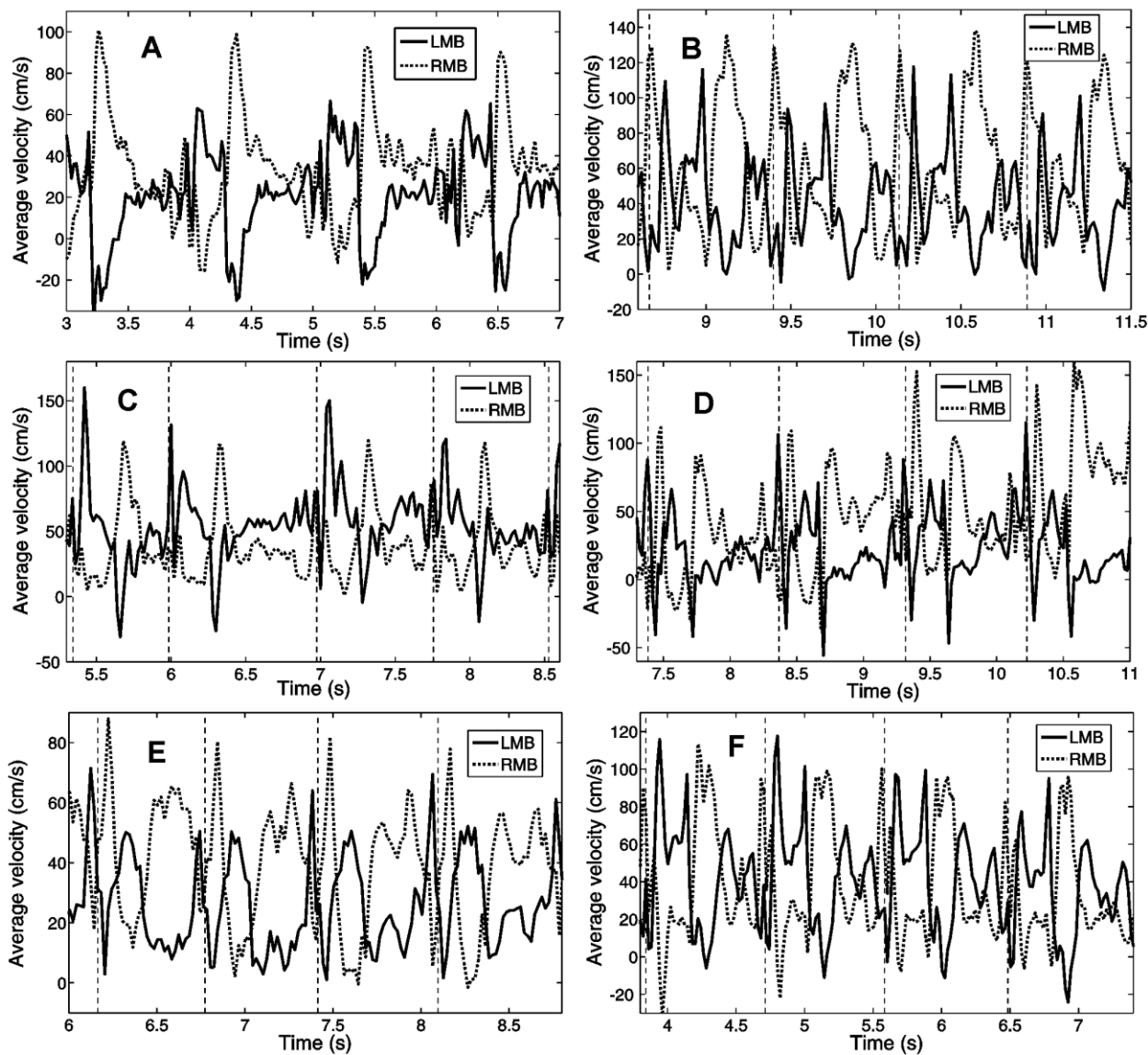
392   **1D PCV**. Time evolution of the average velocity of ^{3}He gas in the left/right main bronchi

393   (LMB/RMB) in subjects 1 to 6 (A to F respectively) during a constant inhalation (see slice

394   location 1 in the inset of Fig. 1). The vertical dashed lines correspond to the occurrences of the

395   R-waves that were recorded with ECG (not recorded for subject 1). For subject 3 (C) a case of

396   arrhythmia can be observed between 6 to 7 s. Mean estimated errors for each average velocity

397   curve were: A LMB: $\pm$ 5 cm s^{-1}; RMB: $\pm$ 5 cm s^{-1}. B LMB: $\pm$ 8 cm s^{-1}; RMB: $\pm$ 7 cm s^{-1}. C LMB:

398   $\pm$ 6 cm s^{-1}; RMB: $\pm$ 5 cm s^{-1}. D LMB: $\pm$ 8 cm s^{-1}; RMB: $\pm$ 6 cm s^{-1}. E LMB: $\pm$ 7 cm s^{-1}; RMB: $\pm$

399   6 cm s^{-1}. F LMB: $\pm$ 5 cm s^{-1}; RMB: $\pm$ 5 cm s^{-1}.
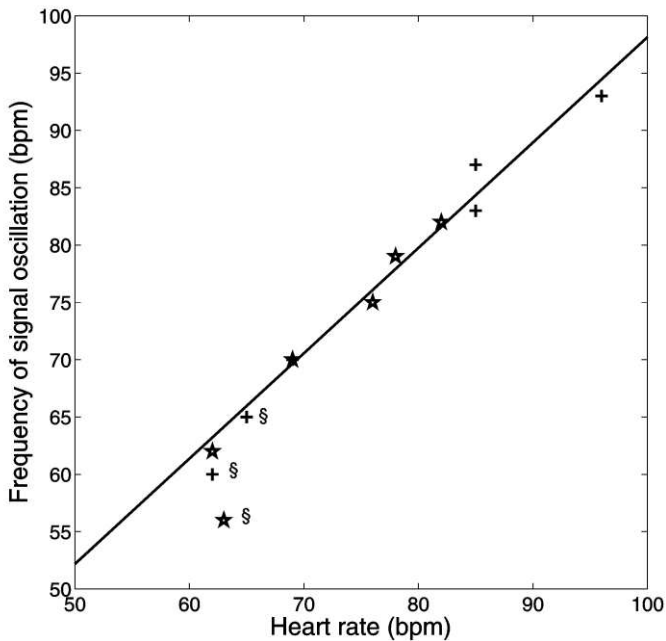
401   Figure 4:

402   Correlation and linear regression line of the fundamental frequency of the signal oscillations and

403   the heart rate measured with ECG. Crosses: from the SNR oscillations of LLL during the

404   dynamic ventilation experiments. Stars: from the 1D velocity measurement (in left main

405   bronchus). Solid line: linear regression line (f(SNR) = 6.24 + 0.92 $\times$ HR, correlation coefficient:

0.99). §: Heart beat measured by finger probe shortly before the experiments and not by

synchronized ECG recording. The three values marked with "§" are shown on the graph but were

not included into the regression line, nor were they used in the calculation of the correlation

coefficient.
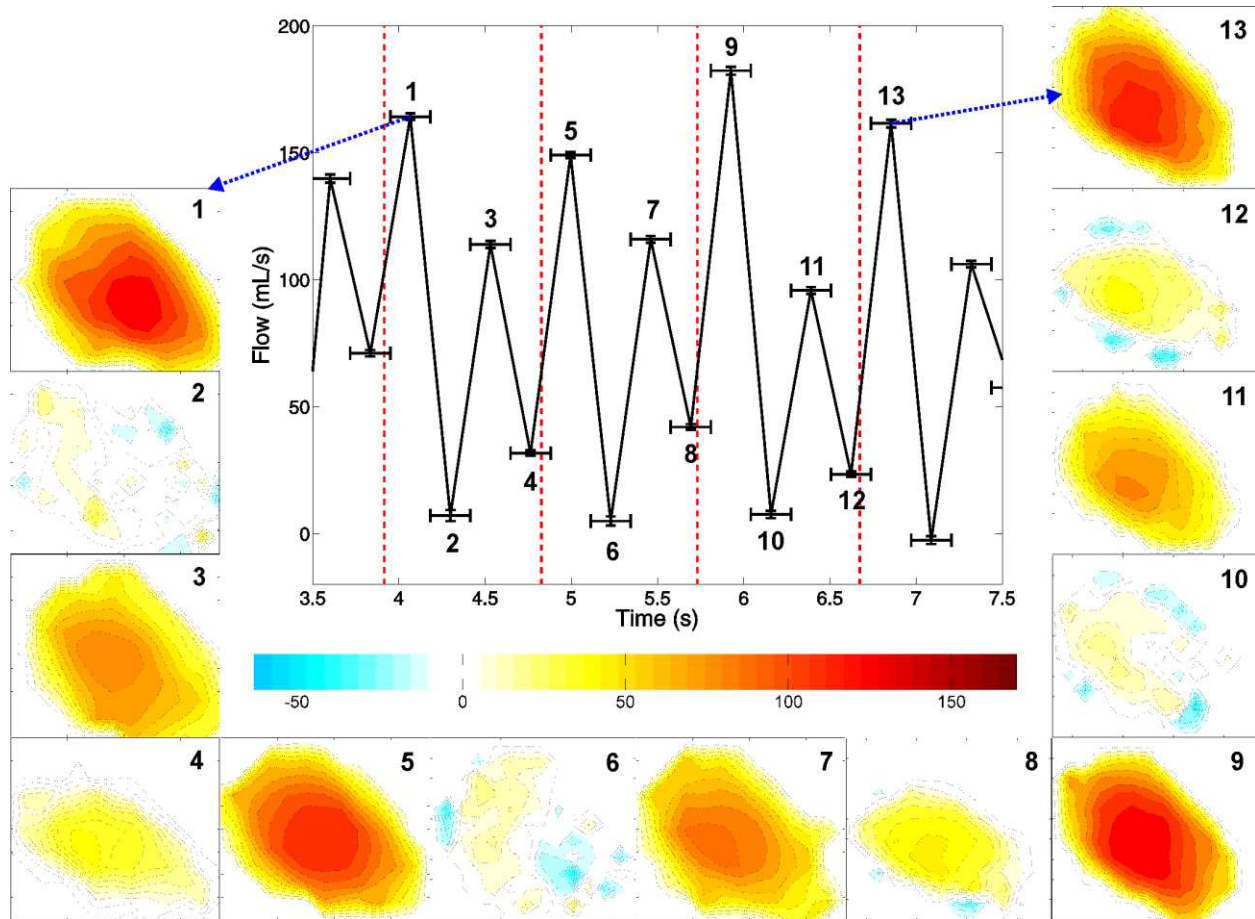
Figure 5:

2D PCV. Time evolution of the ^{3}He gas flow in the left main bronchus of subject 7 measured

during a constant inhalation (see slice location 2 in the inset of Fig. 1, time resolution of 232.4

ms). Example velocity maps (1 - 13), from which the values of the flow curve were calculated,

are shown around the plot (color bar in cm s^{-1}). The average uncertainty σ_v in velocity values for

416   the given velocity maps was ~ 5 cm s^{-1}. The flow error bars (on the vertical axis) were calculated

417   according to the method described in the image analysis section and range between $\pm$ 1 and $\pm$ 2

418   mL s^{-1}. The "x-error bars" on the flow curve represent the acquisition window for each velocity

419   map.
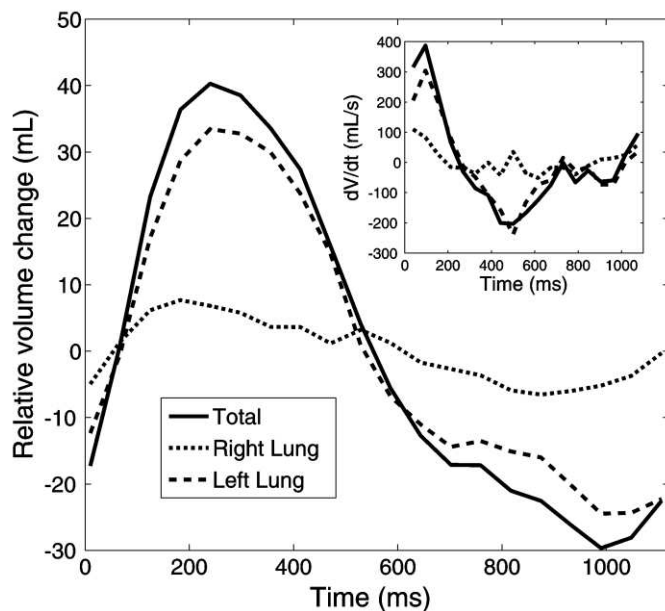
420

421   Figure 6:

422   Relative left and right lung volume changes and the corresponding time-derivatives (inset) after

423   segmentation of a cardiac gated series of proton images of the lungs of subject 1 acquired during

424   breath hold (20 cardiac phases).

425   **Tables**

426   Table 1:

427   Subject characteristics and sequences performed

428   M, male; F, female; FEV$_1$, forced expiratory volume in 1 s; FVC, forced vital capacity. * See ref. (22) . [†]

429   Synchronised ECG recording available.

430   Table 2:

431   Fourier transform analysis of the data from the dynamic ventilation experiments

432   [*] in beats per minute, [†] from finger probe shortly before the experiment, [§] from synchronized ECG
433   recording. [‡] No clear oscillations were observed for subject 5 in the LUL, RLL and RUL explaining why
434   no values are quoted.

435